

# Nanoscale dispersion of palygorskite bundles by a facile mechanical/chemical approach

Wenbo Wang<sup>1,2</sup>, Fangfang Wang<sup>1</sup>, Yuru Kang<sup>1,2</sup>, Li Zong<sup>1,2</sup>, Qin Wang<sup>1,2</sup>, Ai Qin Wang<sup>1,2\*</sup>

<sup>1</sup>Key Laboratory of Clay Mineral Applied Research of Gansu Province, Lanzhou Institute of Chemical Physics, Chinese Academy of Sciences, Lanzhou 730000, P.R. China

<sup>2</sup>R&D Center of Xuyi Palygorskite Applied Technology, Lanzhou Institute of Chemical Physics, Chinese Academy of Science, Lanzhou 730000, P.R. China

\*Corresponding author

DOI: 10.5185/amp.2018/6999

www.vbripress.com/amp

## Abstract

In this paper, we developed a simple mechanical/chemical process to efficiently disperse palygorskite (PAL) crystal bundles into individual nanorods. The “cavity effect” of high-pressure homogenization process generated many “Miniature bombs” in the interior gap of crystal bundles, which may mildly “blast” and effectively burst through the hugged PAL rod crystals without losing their original aspect ratio. Sodium metaaluminate (SM) was simultaneously introduced in the high-pressure homogenization process to promote the dispersion of crystal bundles and restrain the re-aggregation of dispersed nanorods. The dispersion degree and surface charge of PAL nanorods were greatly improved, and the colloidal viscosity of aqueous suspension of highly dispersed PAL rods greatly enhanced by 148% in contrast to raw PAL aggregates. Also, the colloidal stability and rheological properties of PAL were clearly improved after dispersion. As a whole, this process can produce PAL nanorods in an industrial scale, which opens a new avenue to extend the application of PAL in many industrial areas such as fine chemicals, functional carriers and nanocomposites. Copyright © 2018 VBRI Press.

**Keywords:** Palygorskite, high-pressure homogenization, nanoscale dispersion, colloidal properties.

## Introduction

Palygorskite (PAL) is a natural hydrated magnesium-rich silicate clay mineral with rod-like crystal morphology and plentiful nanopores. It has been widely used as colloidal agents [1-3], reinforcing agents [4-7], adsorbents [8-10] and versatile carriers [11, 12], and plays important roles in modern chemical industry. However, the rod crystals in natural PAL mineral are aggregated together due to the hydrogen bonding and Van der Waals forces among rods [13]. Since the bulk aggregates or crystal bundles of PAL do not have the feature of nanomaterials, the disaggregation of PAL crystal bundles as single nanorods is extremely important for its high-value applications.

In general, mechanical treatment is the frequently used method to disaggregate the crystal bundles. With the action of mechanical force, the bulk bundles could be broken up as smaller bundles or individual rods. Thus far, many approaches (i.e., ultrasound, grinding, and extrusion) have been developed to disaggregate the aggregates or bundles of PAL. Darvishi and Morsali [14] employed sonication technology to disperse crude PAL minerals as nanoparticles, and found that the moderate ultrasound action improved the dispersion of PAL rod crystals. Liu *et al.* [15] adopted stone-mill grinding method to disaggregate PAL bundles, and

found that bulk aggregates were dispersed as small aggregates by shearing force, but the PAL nanorods were seriously broken. Boudriche *et al.* [16] studied the effect of different types of dry grinding on the dispersion of PAL. It was found that ball grinding treatment contributes to improve the dispersion of rod crystals, but the fibrous crystal structure was seriously damaged, accompanied by the reduction of particle size. Zhou *et al.* [13] and Wang [17] found that extrusion treatment makes the dense crude PAL mineral become fluffy, which improved the dispersion of PAL in aqueous solution. However, it is contradictory that the disaggregation efficiency is not enough at low-intense extrusion, while the mechanical action may break off the PAL nanorods. The usage of freezing technology may improve the disaggregation efficiency [18], but it is costly, and can't be applied on a large scale in industry. Thus far, there is still no efficient method to disaggregate PAL crystal bundles, with no expense of losing the original aspect ratio of nanorods.

High-pressure homogenization technology has been applied to produce fine emulsion on an industrial scale [19, 20]. The “cavity effect” of homogenization process could transfer force by a special form that is distinct from the traditional mechanical action. The “cavity effect” formed “miniature bomb” in the interior gap of crystal bundles, which may generate strong force from

interior of bundles to exterior. The generated force may overcome the interaction among rods and tear up the crystal bundles. Thus, the nanorods reached an ideal dispersion in liquid phase. However, the dispersed nanorods in solution may re-aggregate as new bundles or aggregates after drying, so that the secondary aggregation problem also needs to be resolved.

Herein, we developed a simple one-step physical/chemical process to disaggregate the crystal bundles and prevent the re-aggregation of dispersed rod crystals. The high-pressure homogenization process effectively disaggregated the crystal bundles, and the simultaneous addition of SM restrained the reaggregation of nanorods. The highly dispersed PAL nanorods were obtained in a form of white powder. The effects of SM dosage on the structure and physicochemical properties of PAL were investigated by Fourier transform infrared spectroscopy (FTIR), Field emission scanning electronic microscopy (SEM), X-ray diffraction (XRD), Zeta potential and BET analyses, and the colloidal properties of the modified PAL were systematically evaluated.

## Experimental

### Materials

Palygorskite (PAL) was taken from the Mingguang mine located on Anhui province of China. Before use, the crude PAL clay mineral was pre-treated by rolled for one times using a three-roller. Sodium meta-aluminate ( $\text{Na}[\text{Al}(\text{OH})_4]$ , AR grade) was purchased from Aladdin Reagent Company (Shanghai, China) and used without further purification. All solutions (or dispersion) were prepared with deionized water.

### Disaggregation and dispersion of PAL crystal bundles

The pretreated PAL (100.0 g) was dispersed in 1400 mL of the aqueous solution containing various amounts of SM (0 g, 0.05 g, 0.10 g, 0.25 and 0.50 g) under continuous mechanical stirring (800 r/min) at room temperature. After stirring for 4 h, the suspension was filtered through a 300-mesh sieve to remove the undesirable large grains of matters. The filtrated suspension was homogenized at 30 MPa on a high-pressure homogenizer (GJB 40-10S, Shanghai Donghua Homogenizer Machinery Corporation, Ltd., Shanghai, China), and then centrifuged at 5000 r/min to separate the solid from the suspension. The solid was dried at 105 °C for 4 h, and then ground and passed through a 200-mesh screen. For a comparison, the SM-modified PAL without homogenization was prepared (coded as SM-0 and SM-0.1). The homogenized samples were coded as SMH-0, SMH-0.05, SMH-0.1, SMH-0.25 and SMH-0.5 according to the dosage of SM.

### Characterizations

XRD patterns were collected on a X'pert PRO X-ray power diffractometer (PAN analytical Co., Netherlands) using  $\text{Cu-K}\alpha$  radiation of 0.1541 nm (40 kV, 30 mA).

The surface morphology was observed using a field emission scanning electron microscope (SEM, JSM-6701F, JEOL) after coating the samples with gold film. FTIR spectra were recorded on a Nicolet NEXUS FTIR spectrometer in 4000-400  $\text{cm}^{-1}$  region using KBr pellets. The specific surface area ( $S_{\text{BET}}$ ) of the samples was determined using the BET method (Micromeritics, ASAP 2010) at 77 K. The BET method was adopted to calculate the specific surface area ( $S_{\text{BET}}$ ), the  $t$ -plot method was adopted to estimate the micropore volumes ( $V_{\text{micro}}$ ). The pore size was calculated from  $PZ = 4V/A$ , where  $V$  is the total volume of pores (obtained from the volume of  $\text{N}_2$  held at the relative pressure  $P/P_0 = 0.95$ ) and  $A$  is the BET surface area. The Zeta potential was measured on a Malvern Zetasizer Nano system with irradiation from a 633 nm He-Ne laser (ZEN3600) at 25 °C, using a folded capillary cell.

### Evaluation of colloidal viscosity and stability

The rotation viscosity was measured at different time and constant shear rate (30 r/min) using a rotational viscosimeter (ZNN-D6, Qingdao Camera Factory, China) with 3<sup>#</sup> spindle. PAL sample (7.0 g) was dispersed in 93 mL of deionized water by high-speed stirring at 11000 rpm for 20 min to obtain homogeneous suspension used for the test of rotation viscosity.

The dispersion stability of PAL suspension was evaluated using a conventional sedimentation method in a graduated cylinder. Typically, 2.5 g of the PAL samples were dispersed in 125 mL of deionized water by high-speed stirring at 11000 rpm for 20 min. The dispersion was transferred to 100 mL graduated cylinder, and then the cylinder was placed in an undisturbed condition for a certain time. The scale indication from the graduated cylinder was recorded as the sedimentation volume of colloidal PAL suspension at fixed time intervals.

### Measurement of rheological behaviors

Shear rheological properties were measured on an Anton Paar Physica MCR301 Rheometer at 25 °C. The shear rate was ranged from 0.1 to 200 1/s. A cone-plate with water bath was used for all measurements. The concentration of the colloidal PAL suspension for test is 7.0 wt% (mass fraction).

## Results and discussion

### XRD analysis

As shown in **Fig. 1**, the characteristic (110) diffraction peaks of PAL were observed at  $2\theta = 8.35^\circ$  ( $d = 1.0589$  nm, for SM-0),  $8.40^\circ$  ( $d = 1.0526$  nm, for SM-0.1),  $8.35^\circ$  ( $d = 1.0589$  nm, for SMH-0),  $8.35^\circ$  ( $d = 1.0589$  nm, for SMH-0.05),  $8.33^\circ$  ( $d = 1.0614$  nm, for SMH-0.1) and  $8.38^\circ$  ( $d = 1.0551$  nm, for SM-0.5), respectively. After the dispersion, the intensity of peaks shows no obvious change. Also, the diffraction peaks at about  $2\theta = 13.75^\circ$  ( $d = 0.6435$  nm, 200 crystal plane),

$2\theta = 16.42^\circ$  ( $d = 0.5394$  nm, 130 crystal plane),  $2\theta = 19.89^\circ$  ( $d = 0.4460$  nm, 040 crystal plane),  $2\theta = 21.48^\circ$  ( $d = 0.4134$  nm, 310 crystal plane),  $2\theta = 24.25^\circ$  ( $d = 0.3667$  nm, 240 crystal plane) [21] do not change obviously, indicating the crystal structure of PAL has not been damaged after dispersion process.

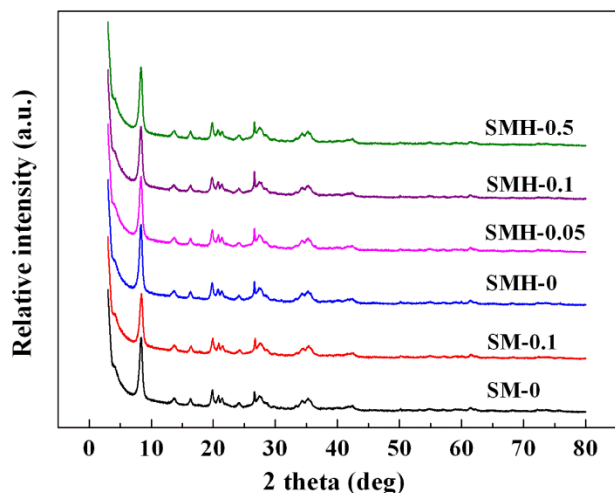


Fig. 1. XRD patterns of crude and dispersed PAL samples.

### SEM morphologies

The SEM micrographs of the PAL samples intuitively reflected the dispersion state of nanorods. As shown in Fig. 2, the rods in crude PAL mineral tightly hugged together to form bulk crystal bundles or aggregates (Fig. 2a). The rods in the bundles or aggregates tend to arrange parallel. After treated with 0.1 wt% SM solution (without homogenization), partial crystal bundles and aggregates were disassociated, but there are still certain amounts of bulk bundles or aggregates, indicating the addition of SM is favorable to improve the dispersion of PAL rods. After treatment with high-pressure homogenization, the number and size of PAL crystal bundles obviously reduced, and the individual nanorods with the size of 0.5-1.5  $\mu\text{m}$  were observed. Simultaneously, the nanorods arrange disorderly (Fig. 2b), indicating high-pressure homogenization process effectively disaggregated the crystal bundles by its special “cavity effect”. After introducing SM during homogenization process, the dispersion of nanorods was improved further (Fig. 2d-f), and the combination of high-pressure homogenization and SM addition may disaggregate the crystal bundles more effectively than single one. It deserves to be noticed that the length of nanorods does not reduce after dispersion, indicating that this method is more superior to the traditional method that may seriously break the nanorods.

Fig. 2g illustrated the proposed mechanism of disaggregation of crystal bundles by “cavity effect” of high-pressure homogenization process. In traditional treatment process, the mechanical force was imposed “from exterior of crystal bundles to interior”, so the force broken the rod crystal. Different from that, the force generated from “cavity effect” mainly act on bundles “from interior to exterior”, and the direction of

force is parallel but reverse with the direction of hydrogen bonding and Van der Waals force. As a result, the force generated from “cavity effect” overcome the hydrogen bonding and Van der Waals force among rods efficiently, so that the disaggregation efficiency is high, and the damage degree of rod crystals is low.

As reported previously [16, 22], after strong mechanical grinding treatment, the intensity of XRD patterns of PAL crystal weakened and the length of nanorods shorten. Comparatively, high-pressure homogenization process can keep the intrinsic aspect ratio of PAL rod after the disaggregation of the bundles into dispersed nanorods. In other word, high-pressure homogenization process is more suitable for the disaggregation of PAL crystal bundles than other mechanical treatments.

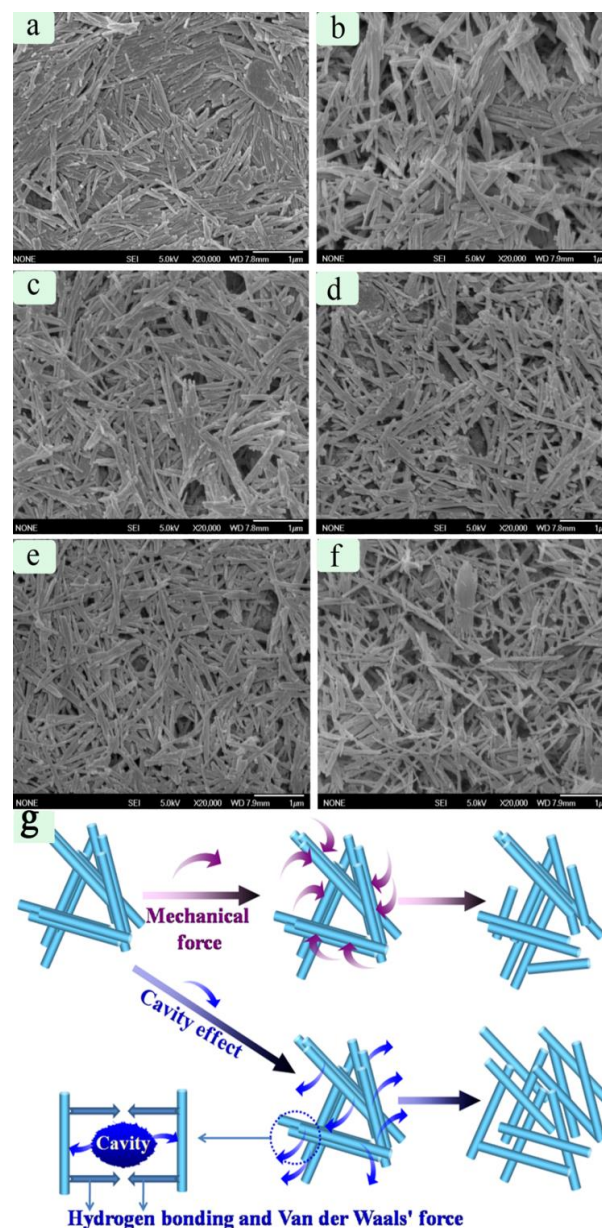


Fig. 2. SEM images of (a) SM-0, (b) SM-0.1, (c) SMH-0, (d) SMH-0.05, (e) SMH-0.1 and (f) SMH-0.5; and (g) proposed mechanism for disaggregation of bundles by “cavity effect”

### FTIR spectra analysis

As shown in the FTIR spectra (Fig. 3), the absorption bands of PAL at 3615  $\text{cm}^{-1}$  (the O-H asymmetric stretching of Al-OH-Al), at 3580  $\text{cm}^{-1}$  (the stretching vibration of O-H in Al-OH-Fe<sup>3+</sup>), at 3551  $\text{cm}^{-1}$  (the asymmetric stretching vibration of O-H of OH<sub>2</sub>), at 3418  $\text{cm}^{-1}$  (the O-H stretching vibration of zeolitic H<sub>2</sub>O), at about 1655  $\text{cm}^{-1}$  (the bending vibration of H-O-H of zeolitic H<sub>2</sub>O), at 1197  $\text{cm}^{-1}$  (the asymmetric stretching vibration of the Si-O-Si bond connected two reverse tetrahedrons), at 1088  $\text{cm}^{-1}$  and 1030  $\text{cm}^{-1}$  (the Si-O absorption bands of SiO<sub>4</sub> moiety), at 982  $\text{cm}^{-1}$  (the stretching vibration of Si-O-Mg), at about 644  $\text{cm}^{-1}$  and 578  $\text{cm}^{-1}$  (the symmetric stretching vibration of H<sub>2</sub>O-Mg-H<sub>2</sub>O and symmetric stretching vibration of AlO<sub>6</sub> octahedron) have no change after dispersion the PAL bundles as rods by the one-step process [23, 24]. This indicates that the crystal structure of PAL has not been destroyed, which is consistent with the XRD and SEM results.

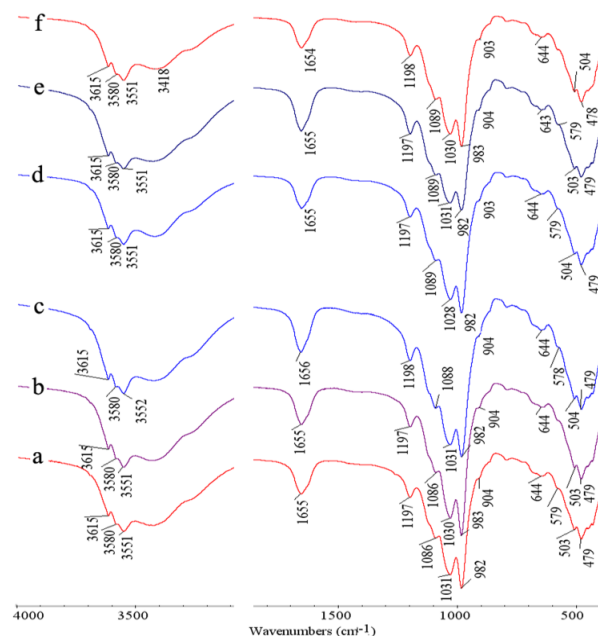


Fig. 3. FTIR spectra of (a) SM-0, (b) SIM-0.1, (c) SMH-0, (d) SMH-0.05, (e) SMH-0.1 and (f) SMH-0.5.

### Zeta potential analysis

Zeta potential may affect the electrostatic interaction between particles and the stability of colloidal solution [25]. As shown in Fig. 4, the Zeta potential of SM-0 sample (without homogenization and SM) is  $-19.5$  mV. After homogenization at 30 MPa or modified with SM (0.1 wt%), the Zeta potentials become negative. After simultaneous treatment with homogenization and SM, the negative Zeta potentials increased to  $-19.9$  mV (for SMH-0.05),  $-20.5$  mV (for SMH-0.1),  $-23.7$  mV (for SMH-0.25) and  $-25.4$  mV (for SMH-0.5), respectively. The negative Zeta potential facilitates to increase the repulsion among rods, and thus prevent the reaggregation of nanorods during drying and improve the dispersion of nanorods.

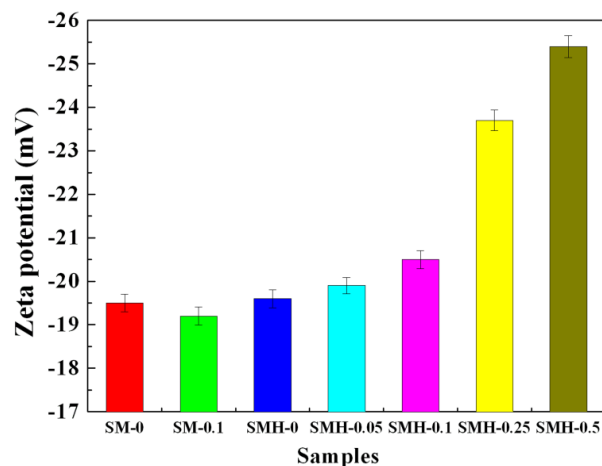


Fig. 4. Zeta potentials of crude and modified PAL.

### BET specific surface areas

Specific surface area ( $S_{\text{BET}}$ ) value of PAL is usually associated with the dispersion degree and aspect ratio of nanorods [26, 27]. As listed in Table 1, the specific surface area ( $S_{\text{BET}}$ ) of crude PAL is 148.3  $\text{m}^2/\text{g}$ , but it increased to 170.7  $\text{m}^2/\text{g}$  after modification with SM (without homogenization). After high-pressure homogenization treatment without adding SM,  $S_{\text{BET}}$  value increased to 204.6  $\text{m}^2/\text{g}$ . This indicates that the modification of PAL with SM and the dispersion of PAL crystal bundles with homogenization enhanced the  $S_{\text{BET}}$  value. Comparatively, the high-pressure homogenization process contributes more to specific surface area than SM modification. The simultaneous physical dispersion and chemical modification increased the  $S_{\text{BET}}$  value more obviously than individual one, and SMH-0.1 sample has the maximum  $S_{\text{BET}}$  (219.4  $\text{m}^2/\text{g}$ ). The increase of  $S_{\text{BET}}$  indicates that the dispersion of PAL nanorods was greatly improved by the physical/chemical approach.

Table 1. Pore structure parameter of raw and modified PAL.

Samples	$S_{\text{BET}}$ ( $\text{m}^2/\text{g}$ )	$S_{\text{micro}}$ ( $\text{m}^2/\text{g}$ )	$V_{\text{micro}}$ ( $\text{cm}^3/\text{g}$ )	PV
SM-0	148.3	12.2	0.0042	0.367
SM-0.1	170.7	35.9	0.0155	0.373
SMH-0	204.6	85.6	0.0450	0.480
SMH-0.05	215.5	88.1	0.0463	0.524
SMH-0.1	219.4	91.8	0.0482	0.533
SMH-0.5	207.5	78.7	0.0412	0.542

The specific surface area of micropores ( $S_{\text{micro}}$ ) sharply increased from 12.2  $\text{m}^2/\text{g}$  (for SM-0) to 91.8  $\text{m}^2/\text{g}$  (for SMH-0.1), indicating that the increase of  $S_{\text{BET}}$  is mainly derived from the exposure of micropores. High-pressure homogenization process may disaggregate effectively the crystal bundles, and the SM may promote disaggregation and restrain the re-aggregation of dispersed nanorods, and so more

micropores were uncovered. As a result, the  $S_{\text{micro}}$  of PAL powder increased. Similarly, the micropore volume ( $V_{\text{micro}}$ ) increased from 0.0042 cm<sup>3</sup>/g (for SM-0) to 0.0482 cm<sup>3</sup>/g (for SMH-0.1). However, excessive addition of SM is adverse to the  $S_{\text{BET}}$  because part of the pores was blocked by excess of SM.

### Rotary viscosity

The viscosity of the aqueous suspension of PAL is closely related to the dispersion degree of rod crystals. As shown in Fig. 5a, the viscosity of aqueous suspension of PAL gradually decreased with increasing shear time, and a typical non-Newtonian fluid feature was observed, indicating the suspension shows good shear-thinning thixotropy. The rotary viscosity of the suspension of SM-0 (without homogenization and SM) is 1812 mPa·s, which decreased to 1228 mPa·s after modification with 0.1% SM (without homogenization), indicating that direct modification of PAL with SM has negative effect on the viscosity. After treatment with high-pressure homogenization, the viscosity of suspension increases to 2356 mPa·s. Intriguingly, synergistic effects were observed after modification of PAL with SM under high-pressure homogenization process. The viscosity sharply increased from 1812 to 2678 mPa·s, enhanced by 47.8%.

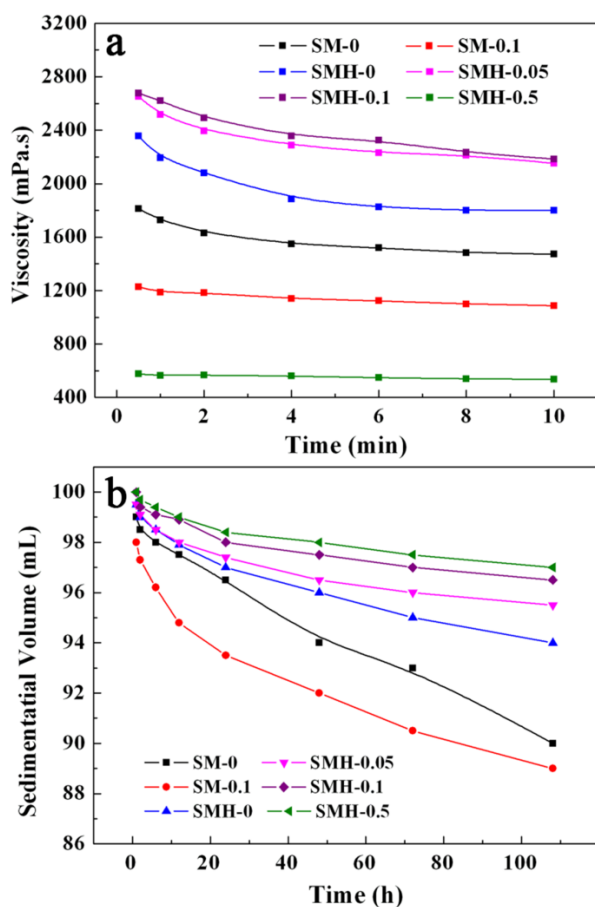


Fig. 5. (a) Rotation viscosity of crude and modified PAL and (b) variation of sedimentation volume of the suspension of crude and modified PAL.

In general, the viscosity of aqueous suspension of PAL is derived from the three-dimensional colloidal network constructed by the “end-to-face” linkage of PAL nanorods *via* electrostatic interaction. The aspect ratio, dispersion degree and surface charges of PAL nanorods decide the viscosity of the colloidal network. After homogenization treatment without adding SM, the viscosity value enhanced due to the well dispersion of nanorods. However, the well dispersed nanorods in aqueous suspension were reaggregated after drying, which induced the loss of colloidal viscosity. The introduction of SM in the process of high-pressure homogenization, the SM may load on the surface of PAL rods and decrease the interaction among rods, which can restrain the re-aggregation of dispersed PAL rods. Thus, PAL rods still have a good dispersion in the dry powder, which can be well dispersed in water to form a stable colloidal network.

However, the excessive addition of SM is adverse to the improvement of rotation viscosity. When the dosage of SM is 0.1 wt%, the viscosity value is only 576 mPa·s. This is resulting from the increase of surface negative charges. The increase of surface charge increased the repulsion among nanorods and makes them tending to arrange parallel, and thus the capability to forming entangled colloidal network decreased.

### Colloidal stability

As shown in Fig. 5b, the aqueous suspension of SM-0 sample (without homogenization and SM) settles down rapidly and the suspending volume is only 89 mL after settling for 108 h. The main reason is that the PAL rods are existed as bundles or aggregates (Fig. 2a), which leads to the rapid settlement of PAL particles in the aqueous suspension under the action of gravitational forces. After homogenization treatment, the suspending volume of PAL suspension was increased to 94.1 mL. The better dispersion of PAL nanorods is favorable to increase the potential energy barrier among the particles that is arisen from the interactions of the electrical double layers and the van der Waals forces and to improve the suspending stability [28, 29]. Whereas, the suspending stability was further improved after introducing SM during homogenization process, and the dosage of SM plays a key role to the suspending stability. The stability was increased with increasing the dosage of SM. This may be ascribed to the fact that, (i) the introduction of SM may effectively restrain the reaggregation of PAL nanorods, and so the resultant powder may easily re-disperse in solvent to form stable colloidal suspension; (ii) the surface charges increased after modifying with SM. The higher surface charges may increase the repulsion among PAL nanorods, and is helpful to the Brownian movement of particle, and then the suspending stability was improved [30]. The improvement of colloidal stability is significant to extend the application of PAL in chemical industries such as coating, paints, daily chemicals.

### Rheological properties

**Fig. 6a** shows the shearing rheological curves of the PAL suspension. It is obvious that the shearing viscosity rapidly decreased with the increase of shear rate, and a typical pseudoplastic flow behavior was observed [31]. The PAL modified with SM *via* high-pressure homogenization process has relatively higher viscosity, and the maximum viscosity at each shear rate was obtained for SM-0.1 sample. The yield stress that the suspension start to flow was evidently observed (**Fig. 6b**). This implies that the association among nanorods increased after the disaggregation of PAL crystal bundles, and so the required stress capable of breaking the clusters of nanorods and orienting the entangled rods to the flow direction increased. Herschel-Bulkley (H-B) model (Eq. 1) [32] is effective to describe the pseudo-plastic flow behavior of a colloidal suspension, and the fitting can be conducted by the method proposed by Coussot and Piau [33].

$$\tau = \tau_0 + m\gamma^a \quad (1)$$

Here,  $\tau$  is shear stress,  $\tau_0$  is yield stress,  $m$  is the consistency coefficient,  $\gamma$  is shear rate, and  $a$  is flow behavior index. The H-B model is usually used for the colloidal suspension that has an initial yield stress at low shear rate, but a pseudoplastic or shear-thinning behavior at a higher shear rate [34]. As shown in **Fig. 6c**, the plots of  $\log(\tau - \tau_0)$  versus  $\log(\gamma)$  exhibit straight lines with good linear correlation coefficients ( $>0.99$ ). The fitting results are listed in **Table 2**. The maximum yield stress of 8.5 Pa was obtained for the SM-0.1 sample. However, the  $\tau_0$  value is only 3.0 Pa for the SM-0.5 sample, which implies that the higher dosage of SM is adverse to the association strength of network due to the increase of repulsion among rods. As shown in **Table 2**, the calculated  $a$  values are smaller than 1, which reveals that the suspension behave not like a Bingham fluid [35]. The value of yield stress is usually to reflect the strength of inter-particle forces in a colloidal suspension, and is an indicator of the amount of stress required to reduce a flocculated system to dispersion. Thus, the colloidal properties of PAL dispersion are closely related to the flocculation degree of the particles and the structure of flocs. The rheological properties of PAL suspension are quite sensitive to the dispersion state of particle and are not apparent until the bundles being separated into individual rods [36]. Thus, the nanoscale dispersion of PAL crystal bundles is the main reason for increase of yield stress.

**Table 2.** The yield stresses of PAL dispersion.

Samples	$\tau_0$ /Pa	$a$	$R^2$
SM-0	6.5	0.4961	0.9961
SM-0.1	5.8	0.2940	0.9968
SMH-0	7.5	0.4490	0.9969
SMH-0.05	8.0	0.3893	0.9979
SMH-0.1	8.5	0.3581	0.9983
SMH-0.5	3.0	0.3258	0.9977

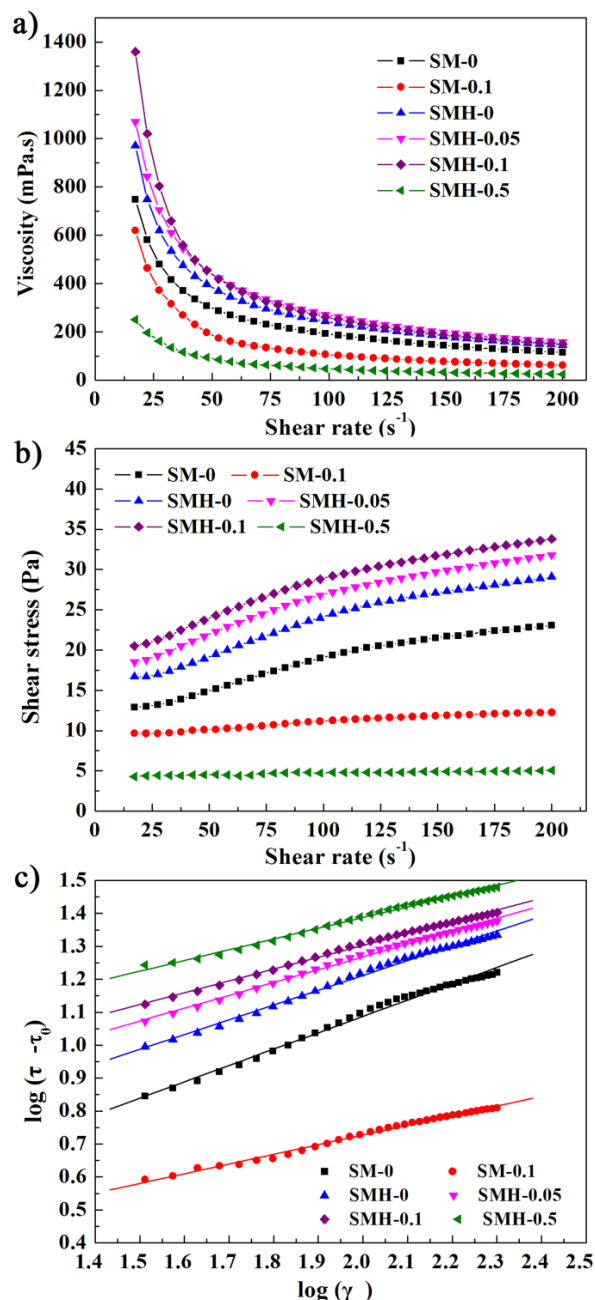


**Fig. 6.** Shearing rheological curves of PAL suspension (a), shear stress curves of PAL suspension (b) and the fitting curves of  $\log(\tau - \tau_0)$  versus  $\log \gamma$  (c).

### Conclusions

PAL has been widely applied in modern industries due to its nanoscale rod-like crystal structure, plentiful nanopores and surface groups. In this work, we developed a simple and industrially available physical/chemical process, and successfully disaggregated the PAL bundles into individual nanorods, with no expense of length of rods. PAL modified with 0.1 wt.% SM and homogenized at 30 MPa gives the best colloidal viscosity and stability, which is superior to that modified by the single one. The surface charges were greatly increased, which is favorable improve the suspension stability; whereas, too high negative charges are not favorable to the

colloidal viscosity. This process is simple but effective, which can be used to produce nanoscale PAL and extend its potential application in modern industry.

#### Acknowledgements

The authors would like to thank “863” Project of the Chinese Ministry of Science and Technology (No. 2013AA032003), the Key Research & Development Project of Gansu Provincial Science and Technology Department, China (17YF1WA167), and the Youth Innovation Promotion Association CAS (2016370) for financial support of this research.

#### Author’s contributions

Conceived the plan: Wenbo Wang, Ai Qin Wang; Performed the experiments: Wenbo Wang, Fangfang Wang, Yuru Kang; Data analysis: Wenbo Wang, Fangfang Wang, Li Zong, Qin Wang; Wrote the paper: Wenbo Wang, Ai Qin Wang, Qin Wang, Li Zong. Authors have no competing financial interests.

#### References

- Baltar, C. A. M.; da Luz, A. B.; Baltar, L. M.; de Oliveira, C. H.; Bezerra, F. J. *Appl. Clay Sci.*, **2009**, *42*(3), 597.  
DOI: [10.1016/j.clay.2008.04.008](https://doi.org/10.1016/j.clay.2008.04.008)
- Neaman, A.; Singer, A. *Appl. Clay Sci.*, **2004**, *25*, 121.  
DOI: [10.1016/j.clay.2003.08.006](https://doi.org/10.1016/j.clay.2003.08.006)
- Liu, Y.; Xu, J.X.; Wang, W.B.; Wang, A.Q. *J. Dispers. Sci. Technol.*, **2014**, *35*, 840.  
DOI: [10.1080/01932691.2013.818547](https://doi.org/10.1080/01932691.2013.818547)
- Ruiz-Hitzky, E.; Darder, M.; Fernandes, F. M.; Wicklein, B.; Alcántara, A.C.S.; Aranda, P. *Prog. Polym. Sci.*, **2013**, *38*, 1392.  
DOI: [10.1016/j.progpolymsci.2013.05.004](https://doi.org/10.1016/j.progpolymsci.2013.05.004)
- Wang, J.H.; Chen, D.J. *J. Nanomater.* **2013**, 496584.  
DOI: [10.1155/2013/496584](https://doi.org/10.1155/2013/496584)
- Chen, L.; Liu, K.; Jin, T. X.; Chen, F.; Fu, Q. *eXPRESS Polym. Lett.*, **2012**, *6*, 629.  
DOI: [10.3144/expresspolymlett.2012.67](https://doi.org/10.3144/expresspolymlett.2012.67)
- Huang, D.J.; Wang, W.B.; Xu J.X.; Wang, A.Q. *Chem. Eng. J.*, **2012**, *210*, 166.  
DOI: [10.1016/j.cej.2012.08.096](https://doi.org/10.1016/j.cej.2012.08.096)
- Sarkar, B.; Megharaj, M.; Xi, Y.F.; Naidu, R. *Chem. Eng. J.*, **2012**, *185–186*, 35.  
DOI: [10.1016/j.cej.2011.05.062](https://doi.org/10.1016/j.cej.2011.05.062)
- Wang, W.B.; Tian, G.Y.; Zhang, Z.F.; Wang, A.Q. *Chem. Eng. J.*, **2015**, *265*, 228.  
DOI: [10.1016/j.cej.2014.11.135](https://doi.org/10.1016/j.cej.2014.11.135)
- Middea, A.; Fernandes, T.L.; Neumann, R.; Gomes O.D.F.; Spinelli, L.S. *Appl. Surf. Sci.*, **2013**, *282*, 253.  
DOI: [10.1016/j.apsusc.2013.05.113](https://doi.org/10.1016/j.apsusc.2013.05.113)
- Wang, W.B.; Wang, F.F.; Kang Y.R.; Wang, A.Q. *RSC Adv.*, **2013**, *3*, 11515.  
DOI: [10.1039/C3RA41836G](https://doi.org/10.1039/C3RA41836G)
- Bouna, L.; Rhouta, B.; Amjoud, M.; Maury, F.; Lafont, M.-C.; Jada, A.; Senocq, F.; Daoudi, L. *Appl. Clay Sci.*, **2011**, *52*, 301.  
DOI: [10.1016/j.clay.2011.03.009](https://doi.org/10.1016/j.clay.2011.03.009)
- Zhou, J.; Liu, N.; Li, Y.; Ma, Y.J. Microstructure characteristics of attapulgite clay. *Bulletin of the Chinese Ceramic Society (Chinese)*, **1999**, *(6)*, 50.
- Darvishi, Z.; Morsali, A. *Appl. Clay Sci.*, **2011**, *51*, 51.  
DOI: [10.1016/j.clay.2010.10.032](https://doi.org/10.1016/j.clay.2010.10.032)
- Liu, Y.; Wang, W.B.; Wang, A.Q. *Powder Technol.*, **2012**, *225*, 124.  
DOI: [10.1016/j.powtec.2012.03.049](https://doi.org/10.1016/j.powtec.2012.03.049)
- Boudriche, L.; Chamayou, A.; Calvet, R.; Hamdi, B.; Balard, H. *Powder Technol.*, **2014**, *254*, 352.  
DOI: [10.1016/j.powtec.2014.01.041](https://doi.org/10.1016/j.powtec.2014.01.041)
- Wang, S. Influence of mechanical squeezing on viscosity of attapulgite (Chinese). *China Non-metallic Mining Industry Herald*, **2005**, *(3)*, 23-24.
- Chen, J.; Jin, Y.; Qian, Y.; Hu, T. *IEEE T. Nanotechnol.*, **2010**, *9*, 6.  
DOI: [10.1109/TNANO.2009.2033675](https://doi.org/10.1109/TNANO.2009.2033675)
- Floury, J.; Desrumaux, A.; Axelos, M.A.V.; Legrand, J. *J. Food Eng.*, **2003**, *58*, 227.  
DOI: [10.1016/S0260-8774\(02\)00372-2](https://doi.org/10.1016/S0260-8774(02)00372-2)
- Xu, J.X.; Zhang, J.P.; Wang, Q.; Wang, A.Q. *Appl. Clay Sci.*, **2011**, *54*, 118.  
DOI: [10.1016/j.clay.2011.07.020](https://doi.org/10.1016/j.clay.2011.07.020)
- Chisholm, J.E. *Can. Mineralogist*, **1992**, *30*, 61.
- Boudriche, L.; Hamdi, B.; Kessaïssia, Z.; Calvet, R.; Chamayou, A.; Dodds, J.A.; Balard, H. *Clay Clay Miner.*, **2010**, *58*, 143.  
DOI: [10.1346/CCMN.2010.0580201](https://doi.org/10.1346/CCMN.2010.0580201)
- Chahi, A.; Petit, S.; decarreau, A. *Clays Clay Miner.*, **2002**, *50*, 306.  
DOI: [10.1346/00098600260358067](https://doi.org/10.1346/00098600260358067)
- Yan, W.C.; Liu, D.; Tan, D.Y.; Yuan, P.; Chen, M. *Spectrochim. Acta A*, **2012**, *97*, 1052.  
DOI: [10.1016/j.saa.2012.07.085](https://doi.org/10.1016/j.saa.2012.07.085)
- White, B.; Banerjee, S.; O'Brien, S.; Turro, N.J.; Herman, I.P. *J. Phys. Chem. C*, **2007**, *111*, 13684.  
DOI: [10.1021/jp070853e](https://doi.org/10.1021/jp070853e)
- Rouquerol, J.; Rouquerol, F.; Llewellyn, P.; Maurin, G.; Sing, K.S. *Adsorption by powders and porous solids: principles, methodology and applications*, Academic Press, 2013.
- Haden, W.L.; Schwint, I.A. *Ind. Eng. Chem.*, **1967**, *59*, 59.
- Rao, F.; Ramirez-Acosta, F.J.; Sanchez-Lejja, R.J.; Song, S.; Lopez-Valdivieso, A. *Appl. Clay Sci.*, **2011**, *51*, 38.  
DOI: [10.1016/j.clay.2010.10.023](https://doi.org/10.1016/j.clay.2010.10.023)
- Zeng, Y.P.; Zimmermann, A.; Aldinger, F.; Jiang, D.L. *J. Eur. Ceram. Soc.*, **2008**, *28*, 2597.  
DOI: [10.1016/j.jeurceramsoc.2008.03.043](https://doi.org/10.1016/j.jeurceramsoc.2008.03.043)
- Eriksson, R.; Kokko, A.; Rosenholm, J.B. *Langmuir*, **2010**, *26*, 7946.  
DOI: [10.1021/ja9048117](https://doi.org/10.1021/ja9048117)
- Van Olphen, H. *An Introduction to Clay Colloid Chemistry*, second ed. John Wiley & Sons, New York, 1977.
- Herschel, W.; Bulkley, R. *Colloid Polym. Sci.*, **1926**, *39*, 291–300.
- Coussot, P.; Piau, J.M. *Rheol. Acta*, **1994**, *33*, 175.
- Luckham, P.F.; Rossi, S. *Adv. Colloid Interf. Sci.*, **1999**, *82*, 43.
- Abu-Jdayil, B. *Int. J. Miner. Process.*, **2011**, *98*, 208.
- Haden Jr, W. L. *Clays Clay Miner.*, **1963**, 284.